Chemical Science

Accepted Manuscript

This article can be cited before page numbers have been issued, to do this please use: J. Du, S. Li, S. Liu, Y. Xin, B. Chen, H. Liu and B. Han, *Chem. Sci.*, 2020, DOI: 10.1039/D0SC01133A.

ROYAL SOCIETY OF CHEMISTRY

rsc.li/chemical-science

View Article Online
DOI: 10.1039/D0SC01133A

ARTICLE

Selective electrochemical reduction of carbon dioxide to ethanol by relay catalytic platform†

Received 00th January 20xx,
Accepted 00th January 20xx

DOI: 10.1039/x0xx00000x

Juan Du,[a,b] Shaopeng Li,[a,b] Shulin Liu,[a,b] Yu Xin,[a,b] Bingfeng Chen,[a] Huizhen Liu,*[a,b] Buxing Han[a,b]

Efficient electroreduction of carbon dioxide (CO_2) to ethanol is of great importance, but this remains a challenge because it involves transfer of multiple proton-electrons and carbon-carbon coupling. Herein, we report a CoO-anchored N-doped carbon material composed of mesoporous carbon (MC) and carbon nanotube (CNT) as a catalyst for CO_2 electroreduction. The faradaic efficiency of ethanol and current density reached 60.1% and 5.1 mA cm^{-2} respectively. Moreover, the selectivity of ethanol products was extremely high among the products produced from CO_2. A proposed mechanism was discussed that the MC-CNT/Co catalyst provided a relay catalytic platform, where CoO catalyze the formation of CO* intermediates which spill over to MC-CNT for carbon-carbon coupling to form ethanol. The high selectivity of ethanol was attributed mainly to the highly selective carbon-carbon coupling active site on MC-CNT.

Introduction

The excessive use of fossil fuels and deforestation result in continuous increase of carbon dioxide (CO_2) concentration in the atmosphere and ocean, which is a crucial issue for human beings.[1] The efficient conversion of CO_2 to fuels and high-value added chemicals can promote the development of the cyclic utilization of carbon resource and the reduction of CO_2 emission.[2, 3] Electrocatalytic reduction of CO_2 is a promising route due to its mild operation conditions (ambient pressure and temperature) and modular reaction systems, which can be easily controlled by adjusting electrochemical parameters and make them facile for scale-up applications.[4-6] Ethanol is a widely used intermediate in chemical synthesis and a liquid fuel with a high energy density (26.8 MJ/kg).[7] Direct electroreduction of CO_2 to ethanol is of great importance. However, it is challenging because the process involves not only the transfer of multiple proton-electrons but also carbon-carbon coupling with high overpotential.

Cu is documented to be a key component for multicarbon chemical production. Unfortunately, most Cu based electrodes is more favorable for ethylene over ethanol. On plasma activated Cu nanocube electrocatalysts, the faradaic efficiency (FE) of ethylene and ethanol were 45% and 22%, respectively.[8] Electrodeposited CuAg alloy films showed good electroreduction performance with FE of 60% for ethylene and 25% for ethanol.[9] Oxide-derived Cu/carbon catalyst exhibited FE of 24% for ethanol production.[10] On bimetallic Ag/Cu electrocatalysts, ethanol could be formed with FE of 41%.[11] The hierarchically structured Cu dendrites electrodes with superhydrophobic surface attained a 56% FE for ethylene and 17% for ethanol production.[12] An ethanol FE of 41% on porphyrin-based Fe/Cu was reported and the ratio of ethanol to ethylene is 1.0 under the optimized operation conditions.[13] Copper-nitrogen-doped carbon materials achieved aqueous CO_2 electroreduction to ethanol at a FE of 55% under optimized conditions.[14] On copper-cuprous oxide electrodes, ethanol and acetic acid could be produced, while the main product is acetic acid.[15]

In addition to the Cu-based electrocatalysts, Ag-, Fe- and carbon materials-based catalysts have also been reported for the electroreduction of CO_2 to ethanol. The Ag-anchored N-doped graphene/carbon foam could efficiently catalyze the conversion of CO_2 to ethanol with FE of 82.1-85.2%, but the current density was only 0.35 mA cm^{-2}.[16] $Fe_2P_2S_6$ nanosheet was used as an efficient electrocatalyst for highly selective electroreduction of CO_2 to methanol and ethanol, with 23.1% FE of ethanol.[17] Ru(II) polypyridyl carbene complex immobilized on an N-doped porous carbon displayed 27.5% FE of ethanol with very low current density.[18] Carbon materials electrodes could catalyze the conversion of CO2 to ethanol with high selectivity while the current density was very low. For example, 77% FE of ethanol was obtained on a nitrogen-doped ordered cylindrical mesoporous carbon with current density of < 1 mA cm^{-2}. Moreover, the selectivity of ethanol among the products produced from CO_2 is nearly 100%.[19] Further study shows that medium micropores embedded in the channel walls of nitrogen-doped ordered mesoporous carbon could promote ethanol production from CO_2 electroreduction, and the FE for ethanol reached 78%.[20]

Literature survey shows that the electrocatalysts that has been reported exhibit high current density and low selectivity for

[a] Beijing National Laboratory for Molecular Sciences, CAS Key Laboratory of Colloid and Interface and Thermodynamics, Institute of Chemistry, Chinese Academy of Sciences, Beijing 100190, P.R. China. E-mail: liuhz@iccas.ac.cn
[b] School of Chemistry and Chemical Engineering, University of Chinese Academy of Sciences, Beijing 100049, P.R. China.
†Electronic Supplementary Information (ESI) available. See DOI:10.1039/x0xx00000x

View Article Online DOI: 10.1039/D0SC01773A

ethanol or high selectivity with low current density. It is obvious that more efforts should be made to develop highly efficient electrocatalysts for the electroreduction of CO_2 to ethanol. CO is an important intermediate for the generation of C_{2+} products from CO_2 electroreduction. It has been reported that high-concentration CO could generate on the doping metal sites and spill over to the Cu sites for carbon-carbon coupling before further reduction to C_{2+} products on Cu-based bimetallic electrodes. Rich local CO intermediates can effectively promote the next carbon-carbon coupling process in CO_2 electroreduction. Moreover, the highly selective carbon-carbon coupling active site on a catalyst are crucial for the electroreduction of CO_2 to ethanol with high selectivity.

Cobalt-based materials can be used as catalysts for electroreduction of CO_2 to CO. On semiconducting Co_3O_4 nanofibers, CO could be formed with FE of 65%.[21] Cobalt phthalocyanine (CoPc) molecules anchored on carbon nanotubes exhibit 95% FE for CO production.[22] Inspired by the high selectivity of carbon materials for CO_2 electroreduction to ethanol and good performance of cobalt-based materials for CO_2 electroreduction to CO, in this work, we designed a catalyst MC-CNT/Co, in which CoO was anchored in N-doped carbon material composed of mesoporous carbon (MC) and carbon nanotube (CNT), for CO_2 electroreduction, which provided a relay catalytic platform, where CoO catalyze the formation of *CO intermediates that spill over to MC-CNT for carbon-carbon coupling to ethanol. The selectivity of ethanol and acetaldehyde could reach nearly 100% among the CO_2 electroreduction products at -0.2 to -0.45 V and a FE of 60.1 % was achieved for ethanol under low overpotential (-0.32 V vs RHE) with the current density of 5.1 mA cm^{-2}. The Co species, ordered mesoporous structure and CNT had excellent synergistic effect for promoting CO_2 electroreduction to ethanol.

Experimental

Reagents

Toray Carbon Paper (CP, TGP-H-60, 19×19 cm), Nafion D-521 dispersion (5 % w/w in water and 1-propanol, ≥ 0.92 meg/g exchange capacity) and Nafion N-117 membrane (0.180 mm thick, ≥ 0.90 meg/g exchange capacity) were purchased from Alfa Aesar China. 3-(Aminopropyl)trimethoxysilane (APTMS), 2-Methylimidazole (purity>98%), Tetraethyl orthosilicate (TEOS) (purity>99%), Cobalt nitrate hexahydrate ($Co(NO_3)_2$) was purchased from Beijing Innochem Company, Pluronic P123 (average Mn ~ 5800) was obtained from Sigma. Hydrochloric acid, Sodium hydroxide, Toluene (purity>99%) was provided by Beijing Chemical Company.

Synthesis of the electrode materials

Preparation of mesoporous silica (MS). The MS was prepared according to the work reported previously.[23] Typically, 4.0 g of Pluronic P123 was dissolved in 50 mL of water and stirred for 5 h at room temperature. The mixture was added to 120 mL of 2 M hydrochloric acid solution and stirred for 2 h, and then TEOS (8.5 g) was added. The solution was aged at 35°C and 100°C for 24 h, respectively. Finally, the solid products were obtained by filteration. Afterwards, the material was washed with deionized water and air-dried overnight. The P123 was removed by calcining in air at 550 °C for 5 h.

Preparation of MS with amino-functional composites (MS-NH_2). 1 g of as-made MS was dispersed in 30 mL of toluene by ultrasonication, and then dropped 2 mL of aminopropyl-methoxysilane (APTMS). The mixture was refluxed at 80 °C with continuous stirring for 24 h. The resulting functionalized MS composites were recovered by filteration followed by washing with toluene several times and then dried at 60°C under vacuum for 12 h. The products obtained are denoted as MS-NH_2.

Synthesis of MC-CNT/Co and MC-CNT. To obtain the MC-CNT/Co, the 2-methylimidazole was used as carbon precursor. In a typical process, Co^{2+}/MS composite template and powder of 2-methylimidazole were mixed to place in quartz boat inside the quartz tube. Ar was introduced as protective and carrier gas. Then the furnace was heated to 700 °C at a rate of 5 °C min^{-1} and kept at the temperature for 3 h to obtain Co/MS/carbon composite. After removing of silica by 10 wt.% NaOH aqueous solution, the MC-CNT/Co was obtained. Moreover, MC-CNT could be obtained by etching metal particles in MC-CNT/Co with hydrochloric acid solution (2 M) for 72 h.

Materials Characterization

The morphologies of those electrodes were characterized on a S4800 scanning electron microscope (SEM) and JEOL-2100F transmission electron microscope (TEM) operated at 200 kV. Powder X-ray diffraction (XRD) patterns were performed on the X-ray diffractometer (Model D/MAX2500, Rigaka) with Cu-Kα radiation. X-ray photoelectron spectroscopy (XPS) analysis was conducted on the Thermo Scientific ESCA Lab 250Xi using 200 W monochromatic Al Kα radiation. The content of Co in the catalysts was determined by inductively coupled plasma optical emission spectroscopy (ICP-OES, Vista-MPX). The N_2 adsorption/desorption isotherms were determined using a Micromeritics TriStar 3020 instrument at -196 °C. The Brunauer-Emmett-Teller (BET) method was employed to calculate the specific surface area, while the Barrett-Joyner-Halenda (BJH) method was applied to analyze the pore size distribution using the adsorption branch of isotherm. The FTIR spectra were collected at a resolution of 4 cm^{-1} on a Bruker Vector 27 spectrophotomfeter in the 400-4000 cm^{-1} region. The IR spectra of samples were measured by the conventional KBr pellet method. Thermogravimetric analysis (Pyris 1 TGA) was performed under Ar flow from 20 to 800 °C at a heating rate of 10 °C min^{-1}.

Electrochemical measurements

The electrochemical workstation (CHI 660E, Shanghai CH Instruments Co., China) was used for all CO_2 reduction experiments. Typically, a 10 mg sample and 20 μL of Nafion solution (5 wt%) were dispersed in 1 mL of deuterium acetonitrile by sonicating for 30 min to form a homogeneous

View Article Online
DOI: 10.1039/D0SC01133A

ink. Then, the dispersion was loaded onto a carbon paper with 1 cm × 1 cm. For CO_2 reduction experiments, cyclic voltammograms (CV) measurements were performed in a H-type cell using 0.5 M $KHCO_3$ (60 mL, pH = 7.8) as electrolyte with a typical three-electrode setup, which contained working electrode, a platinum gauze auxiliary electrode, and an Ag/AgCl reference electrode. All the measured potentials in this work are cited with respect to the RHE using the following conversion: E_{RHE} (V) = $E_{Ag/AgCl}$ (V) + 0.197 V + (0.059 V × pH). Before electrolysis, the electrolyte was purged with Ar or CO_2 gas for at least 30 min. The CV measurement in gas-saturated electrolyte was conducted at a sweep rate of 5 mV s^{-1} in the potential between -0.6 V and -1.4 V (vs. Ag/AgCl). Constant magnetic stirring was kept in the process. The electrolysis experiments were conducted at 25 °C in a typical H-type cell. It consisted of a cathode, an anode (platinum gauze auxiliary electrode) and an Ag/AgCl reference electrode. In the experiments, the cathode and anode compartments were separated by a Nafion-117 proton exchange membrane. $KHCO_3$ aqueous solution (0.5 M) was used as anodic electrolyte. Then, potentiostatic electrochemical reduction of CO_2 was carried out with CO_2 bubbling (5 mL min^{-1}). The reduction of acetaldehyde was also performed over MC-CNT/Co electrode at -0.32 V (vs RHE) in 0.5 M $KHCO_3$ electrolysis solution with 0.05 M acetaldehyde. The electrolysis experiment was conducted at 25 °C in a H-type cell with Nafion-117 proton exchange membrane and lasted 2h. The liquid products were analyzed by ^{1}H NMR (Bruker Avance III 400 HD spectrometer) in Acetonitrile-d3 with dimethyl sulfoxide (DMSO) as an internal standard. The gaseous product was collected using a gas bag and analyzed by gas chromatography (GC, HP 4890D), which was equipped with a TCD detector using helium as the internal standard. Each data point is an average of the measurements collected from at least three separate NMR or GC analysises. Each prepared catalyst was used only once for CO_2 reduction at a chosen potential.

Calculations of Faradaic efficiencies of gaseous and liquid products:

Gaseous products:

FE = moles of products per second/theoretical moles equivalent per second

Based on the GC peak areas and calibration curves, the V % of H_2 can be obtained. The amount of moles of H_2 (or CO) per second could be calculated from the flow rate of the gas and the V % of H_2. The theoretical moles per second were obtained from current density.

liquid products:

In NMR spectra, DMSO was used as the internal standard, and the relative peak area of CH_3CH_2OH can be calculated.
The number of electrons required to produce liquid product during the entire CO_2 electro-reduction reaction is:

$$N = C \times V \times N_A \times n_e$$

(V: the volume of catholyte; N_A: Avogadro constant; n: transfer electron number)

We can obtain the Q_{tatal} from the chronoamperogram and the total number of electrons by measuring,

$$N_{total} = Q_{total} / e$$

The Faradaic efficiency (FE) of liquid product is:

$$FE = N / N_{total} \times 100\%$$

Results and discussion

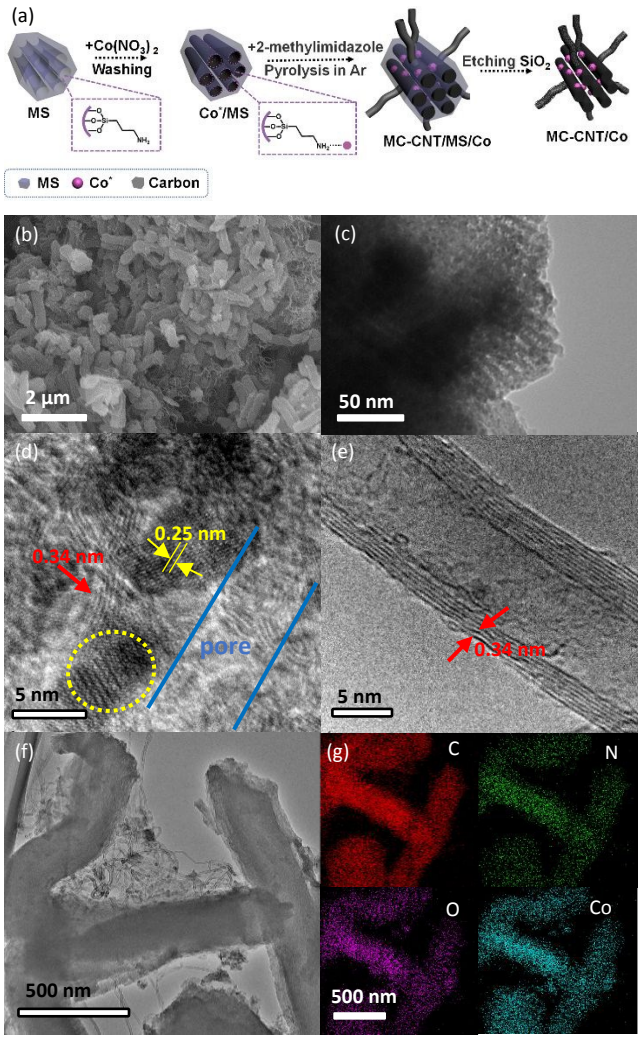

Fig. 1. Schematic illustration of the synthesis process (a), SEM (b), TEM (c and f) images, high-resolution TEM (d and e) and the corresponding elemental mapping of C, O, Co and N elements (g) of the MC-CNT/Co.

Ordered MS was prepared using TEOS as the precursor and P123 as the template. Amino groups were grafted to the MS using APTMS as amination reagent, which was proved by the N-H vibration peaks at 1560 cm^{-1} and 3120 cm^{-1} in the FTIR spectra (Fig. S1). The mesoporous structure of MS was kept after amino

groups grafting (Fig. S2).[24-26] The MC-CNT/Co was synthesized by three steps as shown in Fig. 1a. First, the cobalt species was adsorbed onto the MS to obtain Co^{2+}/MS owing to the electrostatic force between amino and cobalt ion. Second, MC-CNT/Co/MS was obtained by thermal treatment of a mixture composed of Co^{2+}/MS composite and powder of 2-methylimidazole under Ar atmosphere, in which 2-methylimidazole was used as carbon and nitrogen precursor. Subsequently, MC-CNT/Co/MS was treated by 10 wt.% NaOH aqueous solution to remove silica resulting in MC-CNT/Co. SEM and TEM images showed that the MC-CNT/Co had a 3D network structure formed by CNT connected to rod-like mesoporous carbon (Fig. 1b and 1f). As shown in Fig. 1d and 1e, the graphene layers with lattice distance of 0.34 nm could be clearly seen. It has been reported that Co could catalyze the formation of CNT.[27] Ordered mesoporous structure observed from TEM images of MC-CNT/Co displayed that the pores of MS template were replicated (Fig. 1c). Additionally, cobalt nanoparticles (diameter: 3 ～ 5 nm) were also detected, and their lattice spacing was 0.25 nm, which is assigned to CoO (111) (Fig. 1d).[28, 29] The content of cobalt in MC-CNT/Co was 13.20 wt%, which was analyzed by inductively coupled plasma optical emission spectroscopy (ICP-OES). The corresponding elemental mapping reveals its elemental distribution, which shows the uniform N, Co distribution in the carbon framework (Fig. 1g).

Fig. 2a shows the XRD patterns of the MC-CNT/Co. The broad diffraction peaks around 23.3° and 26.0° correspond to the amorphous and graphitized carbon respectively. Three peaks at 36.8°, 43.1° and 63.4° are indexed to the CoO(111), CoO(200) and CoO(220) (CoO-75-0418).[30, 31] As depicted in Fig. 2b, the MC-CNT/Co exhibited type IV adsorption-desorption isotherm and type H3 hysteresis loops, showing the existence of the mesopores. The specific surface area calculated using the BET method was 303 $m^2 g^{-1}$. The BJH method was used to calculate pore-size distribution from the adsorption branch of the nitrogen isotherm and the average pore size was 4.4 nm (Fig. 2c).

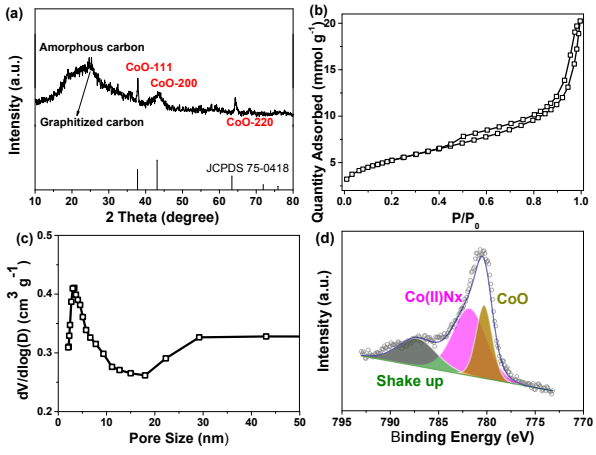

Fig. 2. XRD patterns (a), N_2 adsorption and desorption curves (b), pore size distribution (c) and XPS spectrum of Co2p (d) of the MC-CNT/Co.

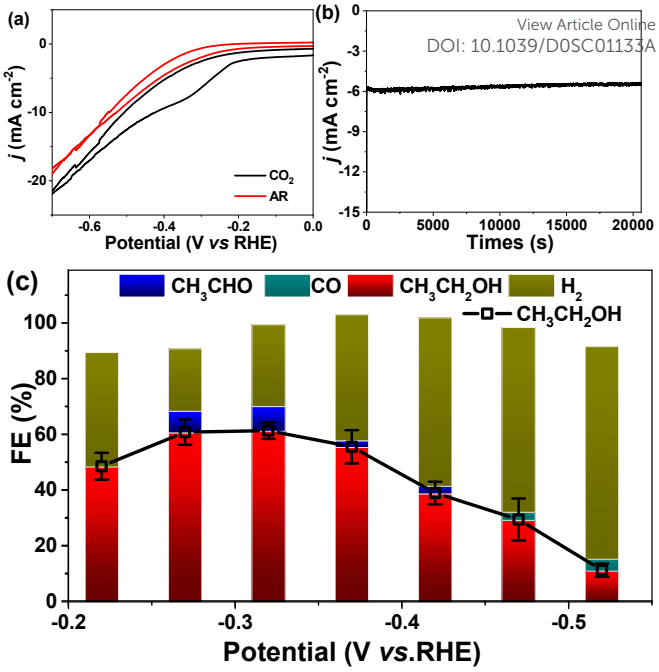

Fig. 3. Cyclic voltammograms curves in the potential range from 0 V to -0.7 V (vs. RHE) at a sweep rate of 5 mV s^{-1} in 0.5 M Ar-saturated and CO_2-saturated 0.5 M $KHCO_3$ on MC-CNT/Co electrodes (a); Total current density versus time in 0.5 M $KHCO_3$ under a CO_2 atmosphere on electrodes at -0.32 V (vs. RHE) (b) and FE for ethanol, aldehyde, carbon monoxide and hydrogen production obtained from the electrochemical reduction of CO_2 for 6 h on MC-CNT/Co electrode at -0.2 to -0.6 V (vs. RHE) (c).

The electronic states of different elements in MC-CNT/Co were investigated by XPS. As shown in Fig. S4, Co, N, C and O elements were observed. The high resolution Co 2p3/2 XPS spectrum of MC-CNT/Co (Fig. 2d) can be deconvoluted into three set peaks at 780.6 eV, 779.3 eV and satellite at 785.5 eV, which are attributed to Co(II)Nx and Co(II)O. [32-34] The O1s signal (Fig. S5a) was deconvoluted into three oxygen configurations, including carboxyl oxygen (532 eV), hydroxyl oxygen (534 eV) in amorphous hydrogenated carbon and Co-O (529 ev).[33] Deconvolution of the N 1s peak (Fig. S5b) revealed two peaks that can be assigned to pyridinic-N (398.5 eV) and pyrrolic-N (400.0 eV), respectively.[34]

The CV tests over MC-CNT/Co were performed in Ar-saturated and CO_2-saturated 0.5 M $KHCO_3$ electrode aqueous solution (pH 7.8) respectively. In this work, the applied potential is referencing to the reversible hydrogen electrode (RHE) and the current density is calculated by geometric surface area. As shown in Fig. 3a, an obvious reduction peak can be observed at ca. -0.3 V (*vs* RHE) in a CO_2-saturated electrolyte, which shows the reduction of CO_2. Controlled-potential CO_2 electrolysis experiments were performed in 0.5 M $KHCO_3$ aqueous electrolyte solution using a typical H type cell. The onset potential of MC-CNT/Co was as low as −0.25 V (*vs* RHE), which is more positive than that of many other carbon-based

View Article Online
DOI: 10.1039/D0SC01972H

electrodes.[19, 35-38] More importantly, ethanol and acetaldehyde (trace) were the only liquid products detected by NMR spectroscopy. H_2 was the only gaseous product in the range of -0.20 to -0.45 V (vs RHE), showing that the selectivity of C_2 liquid products from CO_2 is 100% on the MC-CNT/Co catalyst. The current density and FE for ethanol and acetaldehyde were 5.1 mA cm^{-2} and 70.7% (60.1% for ethanol and 10.0% for acetaldehyde), respectively (Fig. 3b and c). Except for ethanol, a small amount of CO was detected at -0.48 V and -0.52 V (versus RHE), which is a very important intermediate for C2 products as the reported results.[39] MC-CNT/Co exhibited higher FE for ethanol than Cu-based catalysts and higher current density than carbon material-based electrodes. In addition, the MC-CNT/Co catalyst showed long-term stability in the electrolysis, which was known from the fact that both current density and FE did not change considerably with electrolysis time in 20 h at -0.32 V (vs RHE), as shown in Fig. S6.

From the product distribution shown in Fig. 3c, we deduce that acetaldehyde was the possible intermediate to form ethanol. and it can be confirmed by the electroreduction of acetaldehyde. The reduction of acetaldehyde was performed over MC-CNT/Co at -0.32 V (vs RHE) in 0.5 M $KHCO_3$ electrolysis solution (Fig. S7). It can be found that ethanol was produced with 50% conversion and 98% FE.

To confirm that the product was derived from CO_2 reduction, the blank experiments using Ar to replace CO_2 in the electrolysis at -0.3 V vs. RHE (Fig. S8) were conducted and no product was formed after electrolysis 6 h. The reaction in Isotope−labeled $^{13}CO_2$ and $^{12}CO_2$ saturated 0.5 M $KHCO_3$ electrolyte solution at -0.32 V vs RHE was also studied over MC-CNT/Co. The product was analyzed by ^{1}H NMR after electrolysis 1 h. From ^{1}H NMR spectra in Supplementary Fig. S9, we can only see the H signal of $^{13}CH_3$ group on the ethanol, which splits into two peaks by the coupling with ^{13}C atom. The results indicate that carbon atoms in the product were from CO_2 rather than other C-based chemicals in the reaction system.[18, 40]

To unveil the reasons behind the good performance of MC-CNT/Co, MC-CNT and pure CoOx as reference samples for electroreduction of CO_2 were checked. MC-CNT was prepared by etching CoO in MC-CNT/Co with hydrochloric acid solution (2 M) for 72 h, and characterized by TEM, XRD and XPS. Fig. S10 shows CNT and mesopores structure of MC-CNT, and no detectable Co or CoO nano-particles or subnano-clusters were observed. Moreover, no signals of Co or CoO were detected in XRD and XPS spectrum (Fig. S11). These results indicate that Co or CoO was removed by HCl. The pure CoOx sample also prepared by annealing $Co(NO_3)_2$ under Ar atmosphere (Fig. S12). CO_2 electrolysis measurements were performed in CO_2-saturated 0.5 M $KHCO_3$ electrolyte solution using CoOx or MC-CNT as the catalysts and the electrolysis process was carried out at the range of -0.20 to -0.6 V (*vs* RHE) for 2 h. On CoOx electrode, CO was detected with a maximum FE of 5.6% at -0.46 V (*vs* RHE), which is an important intermediate during CO_2 electroreduction to C_2 products (Fig. S13). On MC-CNT electrode, CO and ethanol as result of carbon-carbon coupling were produced with FE of 0.98% and 48.1% at -0.46 V (*vs* RHE), respectively. The pyridinic-N and pyrrolic-N with high electron densities could facilitate the formation of ethanol which is consistent with the results reported in the literature.[19, 20] Furthermore, because of the excellent conductivity of CNT, the current density was measured to be 3.2 mA cm^{-2}, which is higher than the reported carbon electrode. Recent studies have also proved the vital role of CNT in facilitating the electrocatalytic reduction of CO_2.[19, 35, 41, 42] These experimental results suggest that MC-CNT/Co creates a relay catalytic platform that CoOx and MC-CNT cooperate very well to catalyze the formation of C_2 products via CO.

Electrochemical impedance spectroscopy (EIS) was performed at −0.56 V vs. RHE in CO_2 saturated 0.5 M $KHCO_3$ solution to measure the charge transfer resistance (Rct) for MC-CNT/Co and MC-CNT. As shown in Fig. S14, the Rct value of MC-CNT/Co was as low as 0.28 ohm, lower than that of MC-CNT (0.47 ohm), implying that electrons could be more easily transported on MC-CNT/Co.

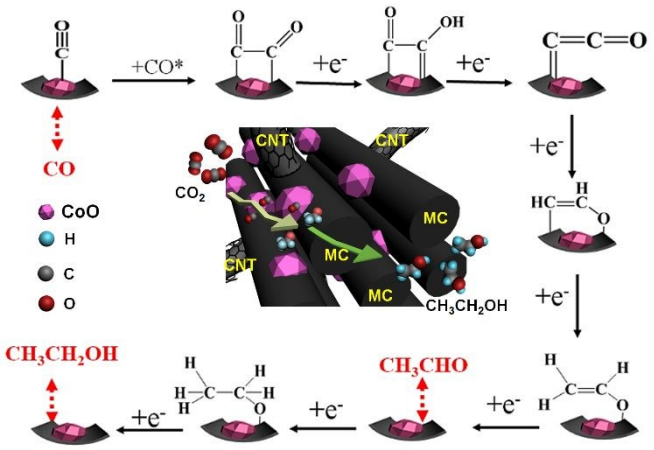

Scheme 1. Proposed mechanism for the electrochemical reduction of CO_2 to ethanol on the MC-CNT/Co electrode.

According to the experimental data and the results have been reported,[35, 43, 44] the possible mechanistic pathway for the electrocatalytic production of ethanol over MC-CNT/Co was proposed and shown in Scheme 1. One-electron transfers to CO_2 molecule to form intermediate CO_2*- anion radical. Subsequently, the obtained CO_2*- reacts with proton-electron pair and forms CO* intermediates, which is mainly attributed to the CoO species. CO* is the key intermediates for the dimerization[35] and it spill over to MC-CNT for carbon-carbon coupling to form *COCHO or *COCO intermediates. Pyrrole-N and pyridinic-N in MC-CNT/Co and its mesoporous structure are both favorable for stabilizing CO* intermediates and promoting the carbon-carbon coupling reaction to ethanol.[19,20] Furthermore, CoO species and MC-CNT are intimate in MC-CNT/Co because it is synthesized by one-pot pyrolysis, which is benefit for the spillover of CO* intermediates to MC-CNT.

DOI: 10.1039/D0SC01133A

Conclusions

In summary, the MC-CNT/Co catalyst designed in this work shows excellent performance for CO_2 electroreduction to ethanol. The FE of ethanol could reach 60.1% at −0.32 V versus the reversible hydrogen electrode. The ordered mesoporous structure and CoO particles cooperate very well to promote the reaction. CoO catalyze the formation of CO* intermediates that spill over to MC-CNT for carbon-carbon coupling to ethanol. Pyrrole-N and pyridinic-N in MC-CNT/Co and its mesoporous structure are both favorable for stabilizing CO* intermediates and promoting the carbon-carbon coupling reaction. The high selectivity of ethanol was attributed mainly to the highly selective carbon-carbon coupling active site on MC-CNT. We believe that relay catalytical platform strategy can also be used for designing highly efficient catalysts for electroreduction CO_2 to C_{2+} products.

Conflicts of interest

There are no conflicts to declare.

Acknowledgements

This work was financially supported by the National Key Research and Development Program of China (2017YFA0403003, 2017YFA0403101), National Natural Science Foundation of China (21871277, 21603235 and 21403248), Beijing Municipal Science & Technology Commission (Z191100007219009), and Chinese Academy of Sciences (QYZDY-SSW-SLH013).

Notes and references

1. X. Duan, J. Xu, Z. Wei, J. Ma, S. Guo, S. Wang, H. Liu and S. Dou, *Adv. Mater.*, 2017, **29**, *1701784*.
2. A. Vasileff, X. Zhi, C. Xu, L. Ge, Y. Jiao, Y. Zheng and S.-Z. Qiao, *ACS Catal.*, 2019, **9**, 9411-9417.
3. L. Lin, H. Li, C. Yan, H. Li, R. Si, M. Li, J. Xiao, G. Wang and X. Bao, *Adv. Mater.*, 2019, **31**, 1903470.
4. H. Yang, Y. w. Hu, J. j. Chen, M. S. Balogun, P. p. Fang, S. Zhang, J. Chen and Y. Tong, *Adv. Energy Mater.*, 2019, **9**, 1901396.
5. D. Gao, I. Sinev, F. Scholten, R. M. Arán-Ais, N. J. Divins, K. Kvashnina, J. Timoshenko and B. R. Cuenya, *Angew. Chem. Int. Ed.*, 2019, *18*, 17047-17053.
6. H. Cui, Y. Guo, L. Guo, L. Wang, Z. Zhou and Z. Peng, *J. Mater. Chem. A*, 2018, **6**, 18782-18793.
7. H. Pramanik and S. Basu, *The Canadian Journal of Chemical Engineering*, 2008, **85**, 781-785.
8. D. Gao, I. Zegkinoglou, N. J. Divins, F. Scholten, I. Sinev, P. Grosse and B. R. Cuenya, *ACS Nano*, 2017, **11**, 4825-4831.
9. T. T. H. Hoang, S. Verma, S. Ma, T. T. Fister, J. Timoshenko, A. I. Frenkel, P. J. A. Kenis and A. A. Gewirth, *J. Am. Chem. Soc.*, 2018, **140**, 5791-5797.
10. K. Zhao, Y. Liu, X. Quan, S. Chen and H. Yu, *ACS Appl. Mater. Interfaces*, 2017, **9**, 5302−5311.
11. Y. C. Li, Z. Wang, T. Yuan, D.-H. Nam, M. Luo, J. Wicks, B. Chen, J. Li, F. Li, F. P. G. d. Arquer, Y. Wang, C.-T. Dinh, O. Voznyy, D. Sinton and E. H. Sargent, *J. Am. Chem. Soc.*, 2019, **141**, 8584-8591.
12. D. Wakerley, S. Lamaison, F. Ozanam, N. Menguy, D. Mercier, P. Marcus, M. Fontecave and V. Mougel, *Nature materials*, 2019, **18**, 1222–1227.
13. F. Li, Y. C. Li, Z. Wang, J. Li, D.-H. Nam, Y. Lum, M. Luo, X. Wang, A. Ozden, S.-F. Hung, B. Chen, Y. Wang, J. Wicks, Y. Xu, Y. Li, C. M. Gabardo, C.-T. Dinh, Y. Wang, T.-T. Zhuang, D. Sinton and E. H. Sargent, *Nature Catal.*, 2020, **3**, 75–82.
14. D. Karapinar, N. T. Huan, N. R. Sahraie, J. Li, D. Wakerley, N. Touati, S. Zanna, D. Taverna, L. H. G. Tizei, A. Zitolo, F. Jaouen, V. Mougel and M. Fontecave, *Angew. Chem. Int. Ed.*, 2019, **58**, 15098 – 15103.
15. Q. Zhu, X. Sun, D. Yang, J. Ma, X. Kang, L. Zheng, J. Zhang, Z. Wu and B. Han, *Nat. Commun.*, 2019, **10**, 3851.
16. K. Lv, Y. Fan, Y. Zhu, Y. Yuan, J. Wang, Y. Zhu and Q. Zhang, *J. Mater. Chem. A*, 2018, **6**, 5025-5031.
17. L. Ji, L. Chang, Y. Zhang, S. Mou, T. Wang, Y. Luo, Z. Wang and X. Sun, *ACS Catal.*, 2019, **9**, 9721−9725.
18. Y. Liu, X. Fan, A. Nayak, Y. Wang, B. Shan, X. Quan and T. J. Meyer, *PNAS*, 2019, **116**, 26353-26358.
19. Y. Song, W. Chen, C. Zhao, S. Li, W. Wei and Y. Sun, *Angew. Chem. In. Ed.*, 2017, **56**, 10840-10844.
20. Y. Song, S. Wang, W. Chen, S. Li, G. Feng, W. Wei and Y. Sun, *ChemSusChem*, 2020, **13**, 293 – 297.
21. A. Aljabour, H. Coskun, D. A. Apaydin, F. Ozel, A. Hassel, P. Stadler, N. S. Sariciftci and M. Kus, *Appl. Catal.*, 2018, **229** 163–170.
22. X. Zhang, Z. Wu, X. Zhang, L. Li, Y. Li, H. Xu, X. Li, X. Yu, Z. Zhang, Y. Liang and H. Wang, *Nat. Commun.*, 2017, **8**, 14675.
23. A. Chen, Y. Yu, R. Wang, Y. Yu, W. Zang, P. Tang and D. Ma, *Nanoscale*, 2015, **7**, 14686-14690.
24. S. H. Huang and D. H. Chen, *J. Hazard. Mater.*, 2009, **163**, 174-179.
25. S. Wang, K. Wang, C. Dai, H. Shi and J. Li, *Chem. Eng. J.*, 2015, **262**, 897-903.
26. L. You, F. Yuan and F. Ma, *J. Phys. Chem. A,* 2015, **89**, 2298-2303.
27. Z. Li, M. Shao, Q. Yang, Y. Tang, M. Wei, D. G. Evans and X. Duan, *Nano Energy*, 2017, **37**, 98-107.
28. K. M. Nam, J. H. Shim, D.-W. Han, H. S. Kwon, Y.-M. Kang, Y. Li, H. Song, W. S. Seo and J. T. Park, *Mater. Chem.*, 2010, **22**, 4446-4454.
29. F. D. Wu and Y. Wang, *J. Mater. Chem.*, 2011, **21**, 6636.
30. Jiaxin Zhao, Zhongcai Shao and H. Zhang, *Mater. Manuf. Processes*, 2020, **35**, 195-201.
31. F. Wu, S. Zhang, B. Xi, Z. Feng, D. Sun, X. Ma, J. Zhang, J. Feng and S. Xiong, *Adv. Energy Mater.*, 2018, **8**, 1703242.
32. W. Hu, Q. Wang, S. Wu and Y. Huang, *J. Mater. Chem. A*, 2016, **4**, 16920-16927.
33. H.-C. Huang, I. Shown, S.-T. Chang, H.-C. Hsu, H.-Y. Du, M.-C. Kuo, K.-T. Wong, S.-F. Wang, C.-H. Wang, L.-C. Chen and K.-H. Chen, *Adv. Funct. Mater.*, 2012, **22**, 3500-3508.
34. H. Wang, X. Bo, A. Wang and L. Guo, *Electrochem. Commun.*, 2013, **36**, 75-79.
35. K. Lv, Y. Fan, Y. Zhu, Y. Yuan, J. Wang, Y. Zhu and Q. Zhang, *J. Mater. Chem. A*, 2018, **6**, 5025-5031.
36. N. Sreekanth, M. A. Nazrulla, T. V. Vineesh, K. Sailaja and K. L. Phani, *Chem. Commun.*, 2015, **51**, 16061-16064.
37. J. Wu, S. Ma, J. Sun, J. I. Gold, C. Tiwary, B. Kim, L. Zhu, N.

View Article Online
DOI: 10.1039/D0SC01133A

Chopra, I. N. Odeh, R. Vajtai, A. Z. Yu, R. Luo, J. Lou, G. Ding, P. J. Kenis and P. M. Ajayan, *Nat. Commun.,* 2016, **7**, 13869.
38. H. Wang, Y. Chen, X. Hou, C. Ma and T. Tan, *Green Chem.*, 2016, **18**, 3250-3256.
39. E. Bertheussen, A. Verdaguer-Casadevall, D. Ravasio, J. H. Montoya, D. B. Trimarco, C. Roy, S. Meier, J. Wendland, J. K. Norskov, I. E. Stephens and I. Chorkendorff, *Angew. Chem. Int. Ed.,* 2016, **55**, 1450-1454.
40. W. M. Brooks, L. N. Moxon, J. Field, M. G. Irving and D. M. Doddrell, *Biochem. Biophys. Res. Commun.*, 1985, **128**, 107-112.
41. Y. Liu, Y. Zhang, K. Cheng, X. Quan, X. Fan, Y. Su, S. Chen, H. Zhao, Y. Zhang, H. Yu and M. R. Hoffmann, *Angew. Chem. Int. Ed.*, 2017, **56**, 15607-15611.
42. Y. Liu, S. Chen, X. Quan and H. Yu, *J. Am. Chem. Soc.*, 2015, **137**, 11631-11636.
43. J. Shen, R. Kortlever, R. Kas, Y. Y. Birdja, O. Diaz-Morales, Y. Kwon, I. Ledezma-Yanez, K. J. Schouten, G. Mul and M. T. Koper, *Nat. Commun.,* 2015, **6**, 8177.
44. I. Ledezma-Yanez, E. P. Gallent, M. T. M. Koper and F. Calle-Vallejo, *Catal. Today*, 2016, **262**, 90-94.

View Article Online
DOI: 10.1039/D0SC01133A

Table of Contents:

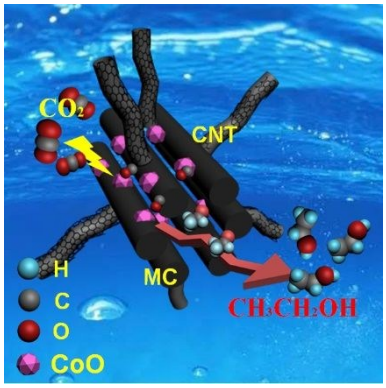

The relay catalytic catalyst is very efficient and selective for CO_2 electroreduction to ethanol through platform.